Advances in Environmental Technology 9(3) 2023, 215-226

Iranian Reasearch Organization for Science and Technology (IROST)

Advances in Environmental Technology

Journal home page: https://aet.irost.ir/

Photocatalytic performance and antibacterial efficacy of green synthesized MgO nanoparticles using *Cymbopogan Citratus*

T.Varghese Nitha, Sebastian Britto

Department of Chemistry, St. Joseph's College (Autonomous), Affiliated to Bharathidasan University,Trichy, Tamil Nadu, India

ARTICLE INFO

Document Type:
Research Paper

Article history:
Received 24 April 2023
Received in revised form
14 August 2023
Accepted 9 September 2023

Keywords:
Green synthesis
MgO nanoparticles
Photocatalysis
Antibacterial activity

ABSTRACT

The current study describes an easy, enviro safe, affordable, and time-saving method to produce Magnesium Oxide (MgO) nanoparticles employing the leaf extract of *Cymbopogon citratus* (Lemon grass) as a reducing and capping agent. X-ray diffraction spectroscopy (XRD), Fourier transform infrared (FT-IR) spectroscopy, scanning electron microscopy (SEM), energy dispersive X-ray spectroscopy (EDX), high-resolution transmission electron microscopy (HR-TEM), photoluminescence spectroscopy (PL), and UV-visible studies were used to characterize the nanoparticles. SEM and TEM analysis of nano MgO revealed that agglomerated particles had nearly spherical morphologies, and the average crystalline size was 25 *nm,* according to the XRD investigation. The bandgap of the synthesized nanoparticles was calculated to be 3.7 eV using a Tauc plot from the UV-visible spectrum. The photocatalytic degradation of the crystal violet (CV) dye in the presence of sunlight was tested, and antibacterial activity was thoroughly investigated for both the Gram-negative (*Escherichia Coli*) and Gram-positive (*Staphylococcus aureus*) pathogens utilizing the MgO nanoparticles. The engineered MgO nanoparticles exhibited excellent utility potential for the photocatalytic degradation of the mentioned dye and antibacterial activity against the two pathogens.

1. Introduction

Environmental contamination, particularly with regard to surface and groundwater resources, represents one of the major problems and concerns of the contemporary world [1]. Industrial and agricultural effluent and contaminants increased significantly as a result of rising industrial activity and population expansion [2]. Both agriculture and the chemical industry employ a variety of chemicals that release poisonous, hazardous molecules into the environment [3]. The dye effluent from the textile sector is one of the primary contaminants that harms both people and the environment [4]. These substances significantly impact humans, including mutagenicity and carcinogenicity; due to this, wastewater must be appropriately purified before

*Corresponding author Tel.: 09656743980
E-mail: nithavarghese89@gmail.com
DOI:10.22104/AET.2023.6187.1703

it is released into the environment [5]. CV dye, which has a structure similar to that of triphenylmethane, is one of the most often used organic dyes and is well known to cause a number of adverse health effects: ocular, respiratory, and digestive tract discomfort. Due to their chemical structural complexity, eliminating them from wastewater discharge is challenging [6]. Removal of these dyes from wastewater is an important matter in the present situation. Water purifying technologies like sedimentation, filtration, chemical, and membrane technologies involve high operation costs with the potential to generate potentially hazardous contaminants in the ecological system [7]. Recent research has demonstrated that an advanced oxidation process can be used to remove dye contaminants from water in place of more traditional techniques because of their cost-effectiveness, simplicity, and efficiency [8]. When semiconductor photocatalysts are exposed to the proper radiation, electron/hole pairs are created, with the electrons being moved into the conduction band and the positive holes remaining in the valence band. Organic pollutants like dyes that are deposited on the semiconductor surface interact with the electron-hole pair and stimulated electrons and holes, which can directly or indirectly generate hydroxyl radicals that degrade organic matter into harmless products like water and carbon dioxide [9,10]. A variety of metal oxides, including ZnO, ZnO/SnO_2, TiO_2, MgO, Fe_3O_4@SiO_2@CeO_2, CuO/Bi_2O_3, etc., have so far been researched for photocatalytic degradation of dye molecules [2,9-11]. MgO nanoparticles have drawn much interest due to their special and distinctive features that could make them useful in catalysis, sensing, medicinal, and biological applications [12]. In light of previous reports, MgO nanoparticles are metal oxide semiconductor photocatalysts that are very efficient for the degradation of methylene blue, methyl orange, methyl red, and rhodamine B [13-16]. There is still a need for more research concerning this nanoparticle in the field of photodegradation. Apart from this, magnesium-based nanoparticles are regarded to be biocompatible, somewhat safer for animals, and essential for plant growth and photosynthesis. The U.S. Food and Drug Administration has approved magnesium-based nanoparticles as a secure alternative with remarkably effective antibacterial properties [17]. The generation of reactive oxygen species in response to light exposure is one of the main antibacterial mechanisms of magnesium oxide NPs [18]. Solution combustion, co-precipitation, sol-gel, hydrothermal, solvothermal, micro-assisted sol-gel, and green approaches are some ways that can be used to create MgO oxide nanoparticles nowadays. Out of all these methods, green synthesis is preferable since it is less expensive, uses fewer harmful chemicals, and produces products and by-products that are environmentally beneficial [19]. It is not necessary to use stabilizers, reductants, or surfactants separately because a variety of phyto molecules found in natural plant extracts work well as reducing, capping, and stabilising agents when NPs are put together [20]. In this respect, extracts from different plants, including Pisidium guvajava, Aloe vera, Trigonella foenum graecum, Clitoria ternatae, and Dalbergia sissoo, have previously been investigated for the purpose of the biosynthesis of MgO nanoparticles [21-24]. In the present investigation, for the first time, an extract from a specific species of Cymbopogan citratus was used for the biosynthesis of MgO nanoparticles. The generated nanoparticles were characterized and employed for antibacterial studies and photocatalytic degradation of crystal violet.

2.Materials and methods

2.1. Chemicals

Mg $(NO_3)_3.6H_2O$ and ethanol were purchased from Merk. The crystal violet dye was bought from the Sigma-Aldrich Chemical Company. *E. coli and S. aureus* were purchased from MTCC, Chandihar, India. The nutrient agar medium and gentamicin antibiotic solution were purchased from Himedia, India.

2.2. Synthesis of plant extract

The fresh lemon grass leaves were collected from Malayattoor (a village in the Ernakulam District, Kerala, South India) and washed carefully with distilled water to eliminate the dust. The leaves were cut into small pieces, dried at room temperature, and made into a fine powder. About 5 gm of the obtained powder was placed into a

beaker, and 100 mL of deionized water was added. The suspension was heated in a water bath to extract the capping agents and subjected to filtration with Whatman No.1 filter paper.

2.3. Synthesis of MgO NPs and instrumentation techniques

The above plant extract (50 mL) was slowly added to a solution of 0.1 M Mg $(NO_3)_3.6H_2O$ (50 mL) in a beaker, stirring constantly (600 rpm) for 2 hr and maintaining the temperature at 80℃. The volume of the mixture was then decreased to 50 mL by keeping it in a hot air oven and initially dried at 180℃ and further annealed at 800℃ in a muffle furnace to afford MgO NPs [22]. The phase structure of the catalyst was recorded by a PANalytical X'Pert PRO Powder X-ray diffractometer with 15 KVA UPS support. FT-IR spectra were recorded with a PERKIN ELMER TWO within a 4000-400 cm^{-1} range. The composition and morphology of the nanostructure were analyzed by SEM with EDAX (TESCAN OXFORD VEGA 3 INCA) and HR-TEM (JEOL Ltd, Tokyo, Japan), respectively. The optical properties of the nano MgO were recorded using Ultraviolet Spectroscopy-LAB INDIA-UV 3092 and Varian Cary Eclipse Photo Luminescence Spectrophotometer, Oxford law temperature LN2 77K arrangement.

2.4. Photocatalytic activity of MgO NPs

The photocatalytic behaviour of the synthesized MgO Nps was assessed by the removal of crystal violet dye under sunlight irradiation. The suspensions of samples were magnetically stirred in the dark for 30 minutes before being exposed to sunlight. The selected dye was used in conjunction with the catalyst sample MgO Nps in different concentrations (.25, .5, .75, and 1g/L) of the photo-removal experiment. Three millilitres of the suspension were collected at periodic time intervals. For the purpose of eliminating the catalyst, the suspension was kept for centrifugation after determining the sample's absorbance using a UV-visible spectrophotometer. The recycling tests were then run four times to check the photocatalyst's stability. Before being used again for the subsequent test, the catalyst used in the experiment was centrifuged, rinsed with ethanol and deionized water, and dried. The photo-removal efficiency percentage was computed using Equation (1):

$$\% \text{ Photo-removal efficiency} = C_0 - C/C_0 \times 100 \quad (1)$$

where C_0 is the initial concentration of dye and C is the concentration of dye after photo-irradiation [25].

2.5. Antibacterial activity of MgO NPs

The agar-well diffusion methodology was employed to evaluate the antibacterial properties of the green-synthesized MgO NPs against the Gram-positive (*S.aureus*) and Gram-negative (*E.coli*) bacteria. The E. coli and S. aureus bacterial strains were seeded in Petri dishes with 20 mL of agar-based nutrient media to conduct a 24-hour cultivation. After piercing the wells, various concentrations of the sample Mg Nps (500□□g□/mL, 250□□g□/mL, 100 □g/mL, and 50□□g□/mL) were administered. The prepared plates were placed in an incubator for twenty-four hours at 37 ˚C. The antibacterial activity was assessed by measuring the diameter of the inhibitory area that formed around the wells. The drug gentamicin served as a positive control [21].

3. Results and discussion

3.1. Structural analysis of nanoparticle

Figure 1 illustrates the results of the XRD investigation done on the MgO-NPs. The relative position of the diffraction peaks in the XRD data revealed that the solid cubic crystal phase was present in the MgO-NPs. The observed diffraction peaks at 2□ values of 36.86°, 42.92°, 62.32°, 74.73°, and 78.49° corresponded to the (hkl) values of (111), (200), (220), (311), and (222), respectively, which showed the cubic structure of MgO-NPs (JCPDS card No. 01-078-0430) [24]. The absence of additional peaks beyond the well-known MgO-NPs diffraction peaks demonstrated that the sample contained no unreacted reactance, and the intended sample did not contain any other contaminants mixed into its crystalline structure. Using the Debye–Scherrer formula, the average crystallite size for these nanomaterials was estimated as 25 *nm*.

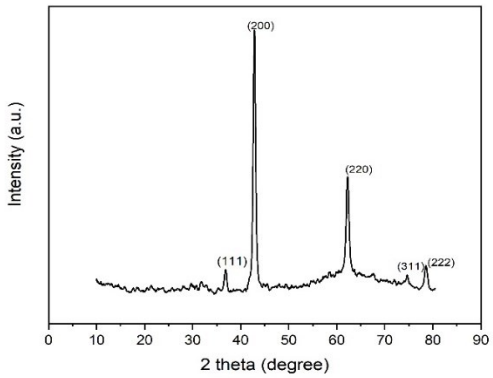

Fig. 1. XRD pattern of MgO NPs.

The bands present in the FTIR spectra (Figure 2) showed the formation of the MgO nanoparticle. The adsorption band at 3422 and 1641 cm^{-1} were responsible for the OH stretching and bending vibrations. The band at 1446 cm^{-1} illustrated the normal absorption pattern of carbonate ions present on this specimen's surface. The Mg-O-Mg (Metal-Oxygen) stretching vibrations correlated to the peak seen between the range of 860-480 cm^{-1} [13].

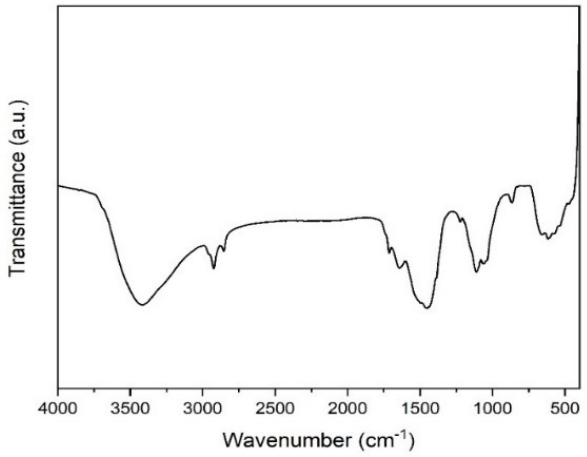

Fig. 2. FT-IR spectrum of MgO NPs.

3.2. Morphological analysis

The SEM and TEM analysis (Figures 3a, 3b, 3d, and 3e) clearly showed that the nanopowders made up of uniform nanostructures consisted of spherical morphology. In the images, it is very evident that the majority of the particles were agglomerated and had rough surfaces. The findings of the elemental compositional analysis conducted with the EDX analyzer were depicted in the EDX spectrum, displayed in Figure 3c. As shown by the EDX spectrum, the produced nanoparticles were clearly made up of magnesium and oxygen. The structure also contained a minor quantity of carbon due to the organic molecules found in the plant extract [22].

3.3. Optical properties of the synthesized nanoparticle

The UV-Vis absorbance spectrum (Figure 4a) for MgO NPs was captured between 200 and 800 nm, and a strong absorption peak was observed at 298 *nm*. Utilizing Tauc's relation, the bandgap energy of the synthesized MgO NPs was ascertained through the UV-visible pattern.

$$(\alpha h\nu)^{n} = A(h\nu - E_g)$$

where α represents the absorption coefficient, *h* is the photon energy, *A* is a constant, E_g is the optical bandgap, and exponent *n* depends on the kind of transition. The synthesized nano MgO was found to have a calculated bandgap energy of 3.71 eV, as demonstrated by the graph of $(\alpha h\nu)^2$ νs hν (Figure 4b), which was smaller than the bandgap energy of bulk MgO (7.8 eV) [26]. The reduced bandgap energy was undoubtedly caused by the presence of 4-coordinated surface anions at the edges of the MgO NPs, whereas 6-coordinated surface anions were present in the bulk materials.

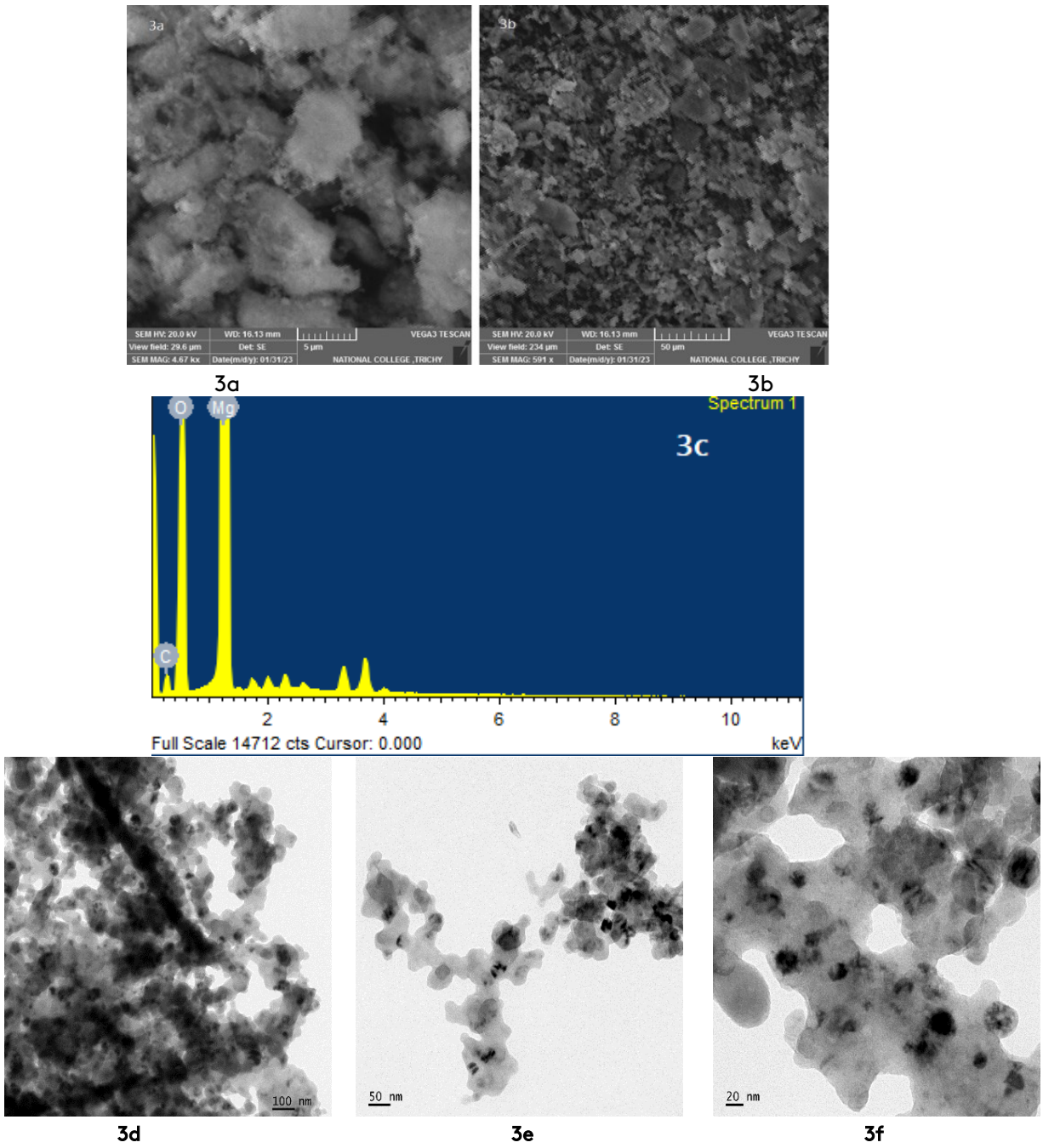

Fig. 3. (a,b) SEM images; **(c)** EDX spectrum; and **(d,e,f)** TEM images.

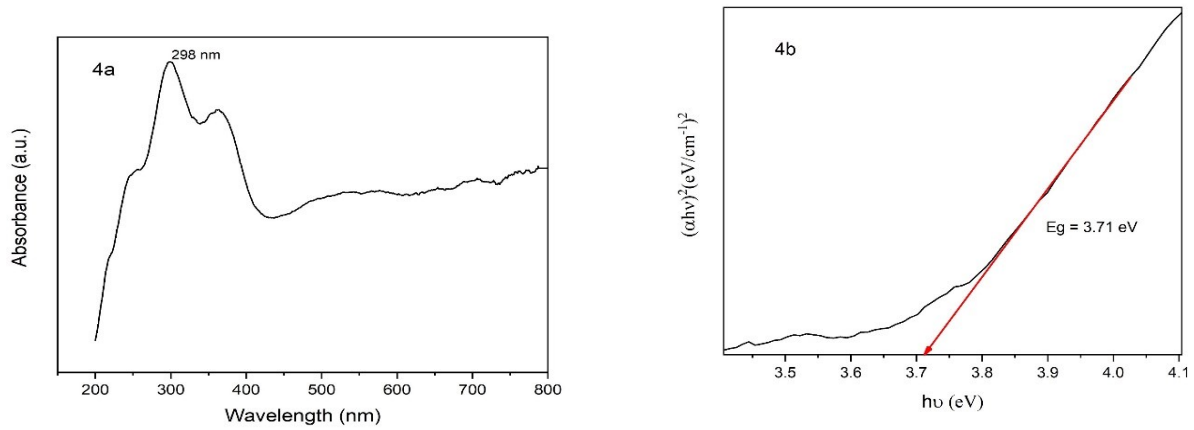

Fig. 4. UV -Visible spectra (a) and Tauc plot (b) of MgO nanoparticle.

Figure 5 displays the PL spectra of MgO NPs. MgO is a common wide-band gap insulator, but due to the existence of inherent imperfections, its PL properties have been explored [27-32]. It should be emphasized that bulk MgO failed to exhibit this luminous spectrum because of the low concentration of surface imperfections [27]. It was obvious that the PL bands in the sample's spectra were not caused by band gap emission but rather by a number of structural defects [28]. The MgO nanostructures frequently displayed luminescence as a result of defects like oxygen vacancies, F-centres (oxygen ion vacancies occupied by two electrons) or F+-centres (oxygen ion vacancies occupied by a single electron), and surface states, the energy levels of which existed in the forbidden energy gap of MgO [29]. The observed emissions in the MgO nanoparticles could be the result of fast evaporation and inadequate crystallization, which could also produce numerous structural flaws [30]. The sample's PL spectrum showed the peak for violet emission at 412 *nm* and blue ejection at 437 and 460 *nm*. Additionally, emission peaks at 360 *nm* were also noted in the spectrum. According to B.H. Niu et al., it is believed that it is caused by scattering from gaps among nanoparticles that are generated at some point during the calcination process [31]. The blue emission peaks are related to structural flaws, including Mg vacancies and interstitials, whereas the violet emission peaks are assigned to the F+ centres in the majority of the MgO [32]. The catalysts with high chemical activity can also originate from the presence of many defect sites, which can also be trapped by oxygen and surface hydroxyl species. The photogenerated electrons and holes in these imperfections also serve as the active sites for photocatalytic activity [14].

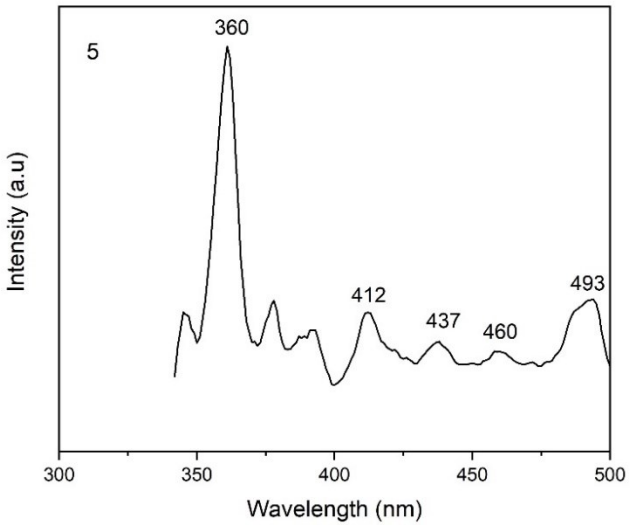

Fig. 5. PL spectrum of MgO.

3.4. Effect of different parameters for the photocatalytic removal of CV dye

For the efficient photocatalytic removal of dye, it is important to find the optimum values for the catalyst quantity, pH, reaction time, and dye concentration. Experiments were conducted to examine the impact of photocatalyst quantity on removal efficiency, with amounts ranging from 0.25 to 1 g/L. In order to speed up the reaction, increasing the amount would increase the number of active sites on the photocatalyst. The removal efficiency of CV was relatively unaffected by increasing the amount of photocatalyst beyond 0.75 g, possibly because of obstacles in the light's passage to the dye molecules. According to Figure

6a, 0.75 g/L was the best concentration for the photocatalyst.

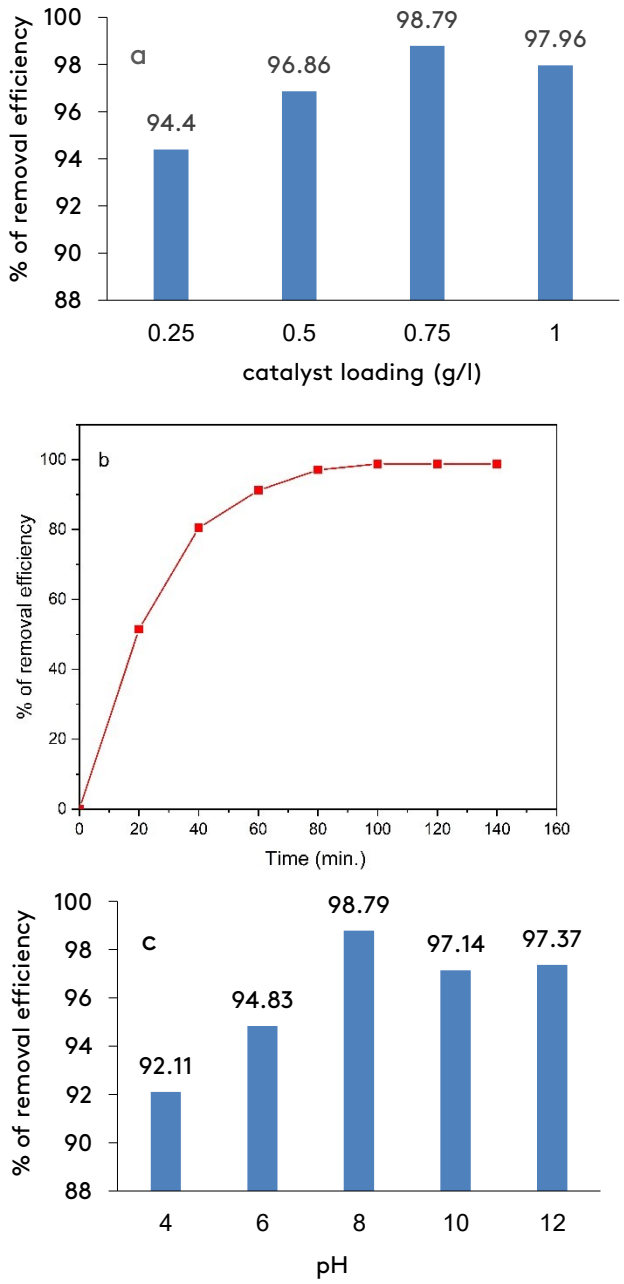

Fig. 6 (a) Effect of catalyst loading on CV removal efficiency. **(b)** Effect of irradiation time on CV removal at pH 8, 0.75 g/L catalyst. **(c)** Effect of pH on CV removal efficiency.

In order to determine the impact of the irradiation period on CV removal efficiency, the solutions were subjected to visible light for up to 140 minutes. Initial high binding rates to sites and rising removal efficiencies were caused by the high concentrations of CV in the solution; these trends leveled off after 100 minutes. For this reason, a response time of 100 minutes was chosen (Figure 6b).

The effectiveness of dye removal was tested in a range of pH values from 4 to 12, with HCl and NaOH used to achieve these values with a 30-ppm dye solution and 0.75 g/L catalyst with 100 minutes of irradiation. The presence of hydroxyl ions caused an increase in the number of negatively charged sites as the pH rose. The photocatalyst and the cation dye created an electrostatic field, improving the efficiency with which CV was removed from the aqueous solution. Figure 6c shows that the largest elimination percentage happened at a pH of 8; hence, that value was chosen as the optimal pH.

The decolorization of crystal violet was examined with respect to dye concentration (Figure 7). The crystal violet dye showed the highest percentage of degradation at a concentration of 30 ppm. An increased degradation rate may be the result of a higher concentration of CV molecules adsorbing on the active site on the surface of the catalyst, which occurred at 30 ppm. Degradation appeared to decrease as the dye concentration rose above 30 ppm, possibly because the catalyst absorbed more dye at high concentrations, preventing irradiation from reaching the catalyst and slowing the decomposition of CV. Based on the above investigation, the optimal conditions for the photodegradation of the CV dye 0.75 g/L catalyst were pH 8 and 30 ppm dye concentration for 100 minutes of irradiation. The comparison of other catalysts with the proposed catalyst is established in Table 1, showing that the proposed catalyst had higher efficiency for removing the mentioned dye in a shorter time.

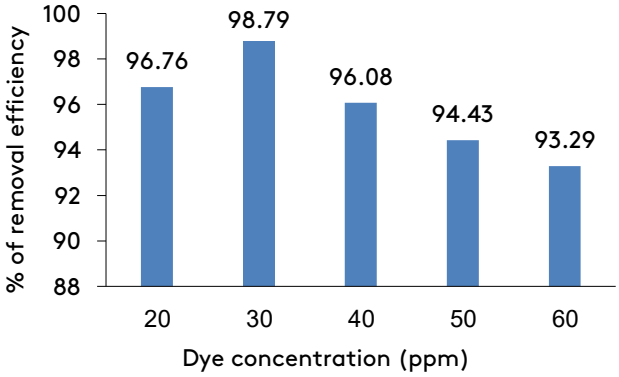

Fig. 7 Effect of dye concentration on CV removal efficiency.

Table 1. Comparison of MgO nanoparticles with other photocatalyst.

No.	Catalyst	Dosage g/L	Dye Concentration (ppm)	Time (min.)	Efficiency (%)	Light Source	Ref.
1	$Ga_2Zr_{2-x}W_xO_7/H_2O_2$	1	10	300	100	Visible Light	[33]
2	Ag^+ doped TiO_2	1	20	105	99	UV Light	[34]
3	Sodium alginate/ZnO/ graphene oxide	1	30	300	94	Sunlight	[35]
4	BiSe-chitosan microsperes	0.2g/20mL	30	150	99.04	Sunlight	[25]
5	$CuCr_2O_4/SnO_2$	1	15	90	100	Sunlight	[36]
6	MgO	0.75	30	100	98.79	Sunlight	PresentWork

3.5. Reusability of catalyst and kinetic study

In this study, the viability and reusability of green-synthesized MgO as a photocatalyst in crystal violet degradation was investigated. Even after four cycles of use, the photocatalyst was still able to remove more than 90% of the CV (Figure 8). This demonstrated the excellent stability of the suggested photocatalyst, which could be reused at least four times without experiencing an apparent decrease in performance.

The kinetics of the photocatalysis was calculated by Equation 2.

$$\ln C_0/C = kt \quad (2)$$

where k is the degradation rate constant and t is the time of degradation [25].

A graph of ln (C_0/C) with time will reveal the apparent rate of activity. Figure 9 indicates that it's quite probable that the reaction was first-order, which was subsequently verified by the linearity of the graph. With a rate constant of K =0.045 min^{-1} and an R^2 of 0.997, the photocatalytic degradation followed pseudo-first-order kinetics. Figure 10 illustrates the schematic representation of photocatalysis.

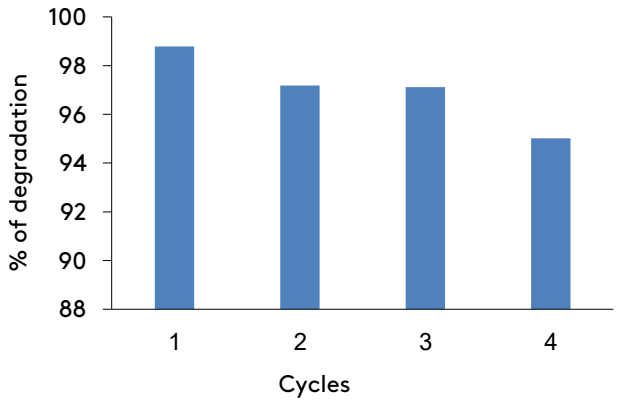

Fig. 8. Reusability of photocatalyst at optimal conditions.

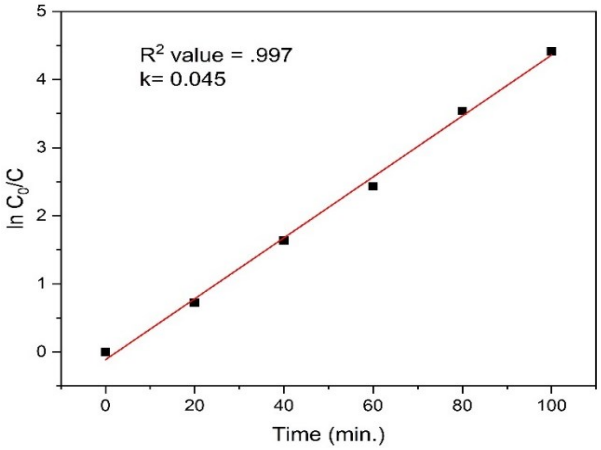

Fig. 9. Kinetic study of CV removal at optimal conditions.

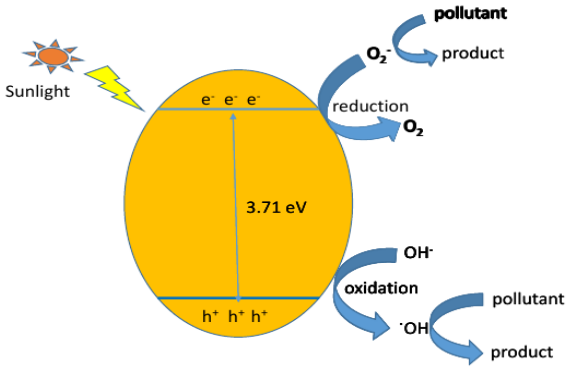

Fig. 10. Schematic representation of photocatalysis.

3.5. Antibacterial properties

The antibacterial properties of MgO nanoparticles are shown in Figure 11. As the solution concentration of MgO NPs increased, the zone of inhibition (ZOI) also increased. Table 2 lists the ZOI of the bacterial species with different concentrations of catalyst; Figure 12 illustrates the ZOI graph against different concentrations of catalyst. The highest MgO NPs concentration of 500 µg/mL formed a ZOI of *18.5±0.7 and 15.5±0.7 for S.aureus* and *E.coli,* respectively. The MgO nanoparticles exposed to UV light caused the development of reactive oxygen species. When ROS were generated, they could cross the bacterial membrane and cause oxidative stress and lipid peroxidation within the bacterial organelles. This oxidative stress weakens the bacterial membrane and can cause cytoplasmic leakage. In addition to their ability to generate ROS, MgO nanoparticles could also bind to bacterial membranes. Since this interaction raised membrane permeability, it was tough for the microorganisms to maintain their essential transport functions appropriately [37].

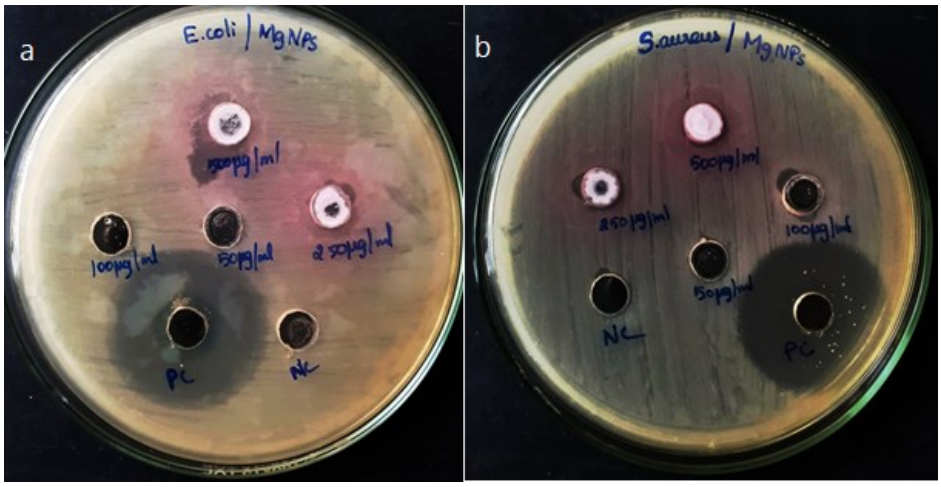

Fig. 11. Inhibition zone of MgO against a) *E.Coli* and b) *S.Aureus*.

Table 2. SD ± Means of zone of inhibition obtained by Sample - MgO Nps against (S. aureus and E. coli).

No.	Organism	Sample	Zone of Inhibition (mm) SD ±Mean				
			PC	500µg/mL	250 µg/mL	100 µg/mL	50 µg/mL
1.	S.Aureus	MgO NPs	22.5±0.7	18.5±0.7	16±1.4	11±1.4	0
2.	E. coli	MgO NPs	16.5±0.7	15.5±0.7	8±1.4	6.5±0.7	0

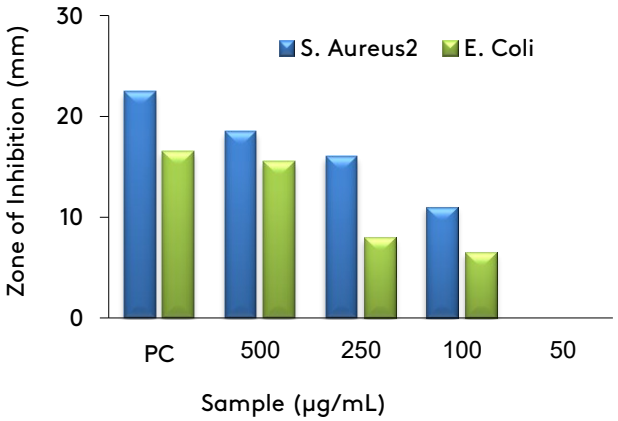

Fig. 12. The measurement of the inhibitory zone at various MgO NPs dosages in the presence of *S. Aureus* and *E. Coli*.

4. Conclusions

In order to protect human health and prevent further damage to the environment, it is necessary that dyes be effectively removed from industrial wastewater and kept out of underground water sources. In this study, the synthesis of MgO nanoparticles using the extract of Cymbopogon citratus was established. The synthesized nanoparticle was characterized by XRD, FTIR, SEM, TEM, EDX, UV, and PL. The proposed photocatalyst showed excellent activity in removing dye contaminants such as crystal violet. Only 0.75 g/L of the nanoparticle was needed to successfully eliminate 98.79% of the dye within 100 minutes when the suspension was exposed to sunlight. It suggests the excellent potential for purifying multi-contaminant water streams. This photocatalytic nanoparticle shows the possibilities for a cost-effective water purification method because it can be reused up to four times without significantly decreasing its photodegradation efficiency. Moreover, the system can offer antibacterial properties as well.

Acknowledgments

administration and principal of St. Joseph's College, (Autonomous), Thiruchirapalli-02 for providing the facilities required to conduct the research.

References

[1] Mangeli, A., Mostafavi, A., Shamspur, T., Fathirad, F., Mehrabi, F. (2021). Decontamination of fenitrothion from aqueous solutions using rGO/MoS_2/Fe_3O_4 magnetic nanosorbent: synthesis, characterization and removal application. *Journal of Environmental Health Science and Engineering*, *19*, 1505-1511. http//doi.org/10.1007/s40201-021-00706-w

[2] Poorsajadi, F., Sayadi, M.H., Hajiani, H., Rezaei, M.R. (2022). Synthesis of CuO/Bi_2O_3 nanocomposite for efficient and recycling photodegradation of methylene blue dye. *International Journal of Environmental Analytical Chemistry*, *102*(18), 7165-7178. http//doi.org/10.1080/03067319.2020.1826464

[3] Shah, N. S., Khan, J. A., Ala'a, H., Sayed, M., Murtaza, B., Khan, H. M. (2016). Synergistic effects of HSO_5– in the gamma radiation driven process for the removal of chlorendic acid: a new alternative for water treatment. *Chemical Engineering Journal*, *306*, 512-521. http//doi.org/10.1016/j.cej.2016.07.031

[4] Li, W., Mu, B., Yang, Y. (2019). Feasibility of industrial-scale treatment of dye wastewater via bio-adsorption technology. *Bioresource Technology*, *277*, 157-170. https://doi.org/10.1016/j.biortech.2019.01.002

[5] Samsami, S., Mohamadizaniani, M., Sarrafzadeh, M. H., Rene, E. R., Firoozbahr, M. (2020). Recent advances in the treatment of dye-containing wastewater from textile industries: Overview and perspectives. *Process Safety and EnvironmentalPprotection, 143*, 138-163. https://doi.org/10.1016/j.psep.2020.05.034

[6] Aggarwal, R., Saini, D., Singh, B., Kaushik, J., Garg, A. K., Sonkar, S. K. (2020). Bitter apple peel derived photoactive carbon dots for the sunlight induced photocatalytic degradation of crystal violet dye. *Solar Energy*, *197*, 326-331. https://doi.org/10.1016/j.solener.2020.01.010

[7] Welderfael, T., Yadav, O. P., Taddesse, A. M., Kaushal, J. (2013). Synthesis, characterization and photocatalytic activities of Ag-N-codoped ZnO nanoparticles for degradation of methyl red. *Bulletin of the Chemical Society of Ethiopia*, *27*(2), 221-232. http//doi.org/10.4314/bcse. v27i2.7

[8] Kargar, F., Bemani, A., Sayadi, M. H., Ahmadpour, N. (2021). Synthesis of modified beta bismuth oxide by titanium oxide and highly efficient solar photocatalytic properties

on hydroxychloroquine degradation and pathways. *Journal of Photochemistry and Photobiology A: Chemistry*, *419*, 113453. http//doi.org/10.1016/j.jphotochem.2021.113453

[9] Sayadi, M. H., Ghollasimood, S., Ahmadpour, N., Homaeigohar, S. (2022). Biosynthesis of the ZnO/SnO_2 nanoparticles and characterization of their photocatalytic potential for removal of organic water pollutants. *Journal of Photochemistry and Photobiology A: Chemistry*, *425*, 113662. https://doi.org/10.1016/j.jphotochem.2021.113662

[10] Fathirad, F., Ziaadini, F., Mostafavi, A., Shamspur, T. (2021). Three-layer magnetic nanocomposite containing semiconductor nanoparticles as catalyst for dye removal from water solutions under visible light. *Iranian Journal of Chemistry and Chemical Engineering*, *40*(6), 1749-1756. https://doi.org/10.30492/IJCCE.2020.122646.4012

[11] Kumari, V., Mittal, A., Jindal, J., Yadav, S., Kumar, N. (2019). S-, N-and C-doped ZnO as semiconductor photocatalysts: A review. *Frontiers of Materials Science*, *13*, 1-22. https://doi.org/10.1007/s11706-019-0453-4

[12] Khan, M. I., Akhtar, M. N., Ashraf, N., Najeeb, J., Munir, H., Awan, T. I., Kabli, M. R. (2020). Green synthesis of magnesium oxide nanoparticles using Dalbergia sissoo extract for photocatalytic activity and antibacterial efficacy. *Applied Nanoscience*, *10*, 2351-2364. https://doi.org/10.1007/s13204-020-01414-x

[13] Balakrishnan, G., Velavan, R., Batoo, K. M., Raslan, E. H. (2020). Microstructure, optical and photocatalytic properties of MgO nanoparticles. *Results in Physics*, *16*, 103013. https://doi.org/10.1016/j.rinp.2020.103013

[14] Mageshwari, K., Mali, S. S., Sathyamoorthy, R., Patil, P. S. (2013). Template-free synthesis of MgO nanoparticles for effective photocatalytic applications. *Powder Technology*, *249*, 456-462. https://doi.org/10.1016/j.powtec.2013.09.016

[15] Ratnam, M.V., Karthikeyan, C., Rao, K.N. Meena, V. (2020). Magnesium oxide nanoparticles for effective photocatalytic degradation of methyl red dye in aqueous solutions: Optimization studies using response surface methodology. *Materials Today: Proceedings*, 26, 2308-2313. https://doi.org/10.1016/j.matpr.2020.02.498

[16] Pachiyappan, J., Gnanansundaram, N., Sivamani, S., Sankari, N.P.B.P., Senthilnathan, N., Kerga, G.A. (2022). Preparation and Characterization of Magnesium Oxide Nanoparticles and Its Application for Photocatalytic Removal of Rhodamine B and Methylene Blue Dyes. *Journal of Nanomaterials*, 6484573. https://doi.org/10.1155/2022/6484573

[17] Pathania, D., Kumar, S., Thakur, P., Chaudhary, V., Kaushik, A., Varma, R. S., Khosla, A. (2022). Essential oil-mediated biocompatible magnesium nanoparticles with enhanced antibacterial, antifungal, and photocatalytic efficacies. *Scientific Reports*, *12*(1), 11431. https://doi.org/10.1038/s41598-022-14984-3

[18] Gold, K., Slay, B., Knackstedt, M., Gaharwar, A. K. (2018). Antimicrobial activity of metal and metal-oxide based nanoparticles. *Advanced Therapeutics*, *1*(3), 1700033. https://doi.org/10.1002/adtp.201700033

[19] S. Abinaya, Helen P. Kavitha, M. Prakash, A. Muthukrishnaraj. (2021). Green synthesis of magnesium oxide nanoparticles and its applications: A review. *Sustainable Chemistry and Pharmacy*,19,100368. https://doi.org/10.1016/j.scp.2020.100368

[20] Pathania, D., Kumar, S., Thakur, P., Chaudhary, V., Kaushik, A., Varma, R. S., Khosla, A. (2022). Essential oil-mediated biocompatible magnesium nanoparticles with enhanced antibacterial, antifungal, and photocatalytic efficacies. *Scientific Reports*, *12*(1), 11431. https://doi.org/10.1038/s41598-022-14984-3

[21] Umaralikhan, L., Jamal Mohamed Jaffar, M. (2018). Green synthesis of MgO nanoparticles and its antibacterial activity. *Iranian Journal of Science and Technology, Transactions A: Science*, *42*, 477-485. http://dx.doi.org/10.1007/s40995-016-0041-8

[22] Vergheese, M., Vishal, S. K. (2018). Green synthesis of magnesium oxide nanoparticles

using Trigonella foenum-graecum leaf extract and its antibacterial activity. *Journal of Pharmacognosy and Phytochemistry*, *7*(3), 1193-1200. https://www.phytojournal.com/archives/2018.v7.i3.4326.

[23] John Sushma, N., Prathyusha, D., Swathi, G., Madhavi, T., Deva Prasad Raju, B., Mallikarjuna, K., Kim, H. S. (2016). Facile approach to synthesize magnesium oxide nanoparticles by using Clitoria ternatea—characterization and in vitro antioxidant studies. *Applied Nanoscience*, *6*, 437-444. http://dx.doi.org/10.1007/s13204-015-0455-1

[24] Khan, M. I., Akhtar, M. N., Ashraf, N., Najeeb, J., Munir, H., Awan, T. I., Kabli, M. R. (2020). Green synthesis of magnesium oxide nanoparticles using Dalbergia sissoo extract for photocatalytic activity and antibacterial efficacy. *Applied Nanoscience*, *10*, 2351-2364. http://dx.doi.org/10.1007/s13204-020-01414-x

[25] Ahmad, W., Khan, A., Ali, N., Khan, S., Uddin, S., Malik, S., Bilal, M. (2021). Photocatalytic degradation of crystal violet dye under sunlight by chitosan-encapsulated ternary metal selenide microspheres. *Environmental Science and Pollution Research*, *28*, 8074-8087. https://doi.org/10.1007/s11356-020-10898-7

[26] Somanathan, T., Krishna, V. M., Saravanan, V., Kumar, R., Kumar, R. (2016). MgO nanoparticles for effective uptake and release of doxorubicin drug: pH sensitive controlled drug release. *Journal of Nanoscience and Nanotechnology*, *16*(9), 9421-9431. https://doi.org/10.1166/jnn.2016.12164

[27] Kumar, N., Sanyal, D., Sundaresan, A. (2009). Defect induced ferromagnetism in MgO nanoparticles studied by optical and positron annihilation spectroscopy. *Chemical Physics Letters*, *477*(4-6), 360-364. https://doi.org/10.1016/j.cplett.2009.07.037

[28] Lu, H. B., Liao, L., Li, H., Tian, Y., Wang, D. F., Li, J. C., Wu, Y. (2008). MgO nanobelts using a reactive and auto-removed ZnO nanobelt template. *Solid State Communications*, *147*(1-2), 57-60. https://doi.org/10.1016/j.ssc.2008.04.019

[29] Jin, C., Kim, H., An, S., Lee, C. (2012). Photoluminescence properties of Sn-embedded MgO nanorods with different morphologies synthesized by a single thermal evaporation process. *Chemical Engineering Journal*, *198*, 420-425. https://doi.org/10.1016/j.cej.2012.05.096

[30] Selvam, N. C. S., Kumar, R. T., Kennedy, L. J., Vijaya, J. J. (2011). Comparative study of microwave and conventional methods for the preparation and optical properties of novel MgO-micro and nano-structures. *Journal of Alloys and Compounds*, *509*(41), 9809-9815. https://doi.org/10.1016/j.jallcom.2011.08.032

[31] Niu, H., Yang, Q., Tang, K., Xie, Y. (2006). Self-assembly of porous MgO nanoparticles into coral-like microcrystals. *Scripta Materialia*, *54*(10), 1791-1796. https://doi.org/10.1016/j.scriptamat.2006.01.036

[32] Kim, H. W., Shim, S. H. (2006). Growth of MgO nanowires assisted by the annealing treatment of Au-coated substrates. *Chemical Physics Letters*, *422*(1-3), 165-169. https://doi.org/10.1186/1556-276X-6-566

[33] Abbas, H. A., Nasr, R. A., Abu-Zurayk, R., Al Bawab, A., Jamil, T. S. (2020). Decolourization of crystal violet using nano-sized novel fluorite structure Ga2Zr2− x W x O7 photocatalyst under visible light irradiation. *Royal Society Open Science*, *7*(3), 191632. https://doi.org/10.1098/rsos.191632

[34] Sahoo, C., Gupta, A. K., Pal, A. (2005). Photocatalytic degradation of Crystal Violet (CI Basic Violet 3) on silver ion doped TiO_2. *Dyes and Pigments*, *66*(3), 189-196. https://doi.org/10.1016/j.dyepig.2004.09.003

[35] Mohamed, S. K., Hegazy, S. H., Abdelwahab, N. A., Ramadan, A. M. (2018). Coupled adsorption-photocatalytic degradation of crystal violet under sunlight using chemically synthesized grafted sodium alginate/ZnO/graphene oxide composite. *International Journal of Biological Macromolecules*, *108*, 1185-1198. https://doi.org/10.1016/j.ijbiomac.2017.11.028

[36] Lahmar, H., Benamira, M., Douafer, S., Akika, F. Z., Hamdi, M., Avramova, I., Trari, M. (2020). Photocatalytic degradation of crystal violet dye on the novel $CuCr_2O_4/SnO_2$ hetero-system under sunlight. *Optik*, *219*, 165042.

https://doi.org/10.1016/j.ijleo.2020.165042
[37] Gold, K., Slay, B., Knackstedt, M., Gaharwar, A. K. (2018). Antimicrobial activity of metal and metal-oxide based nanoparticles. *Advanced Therapeutics*, *1*(3), 1700033. https://doi.org/10.1002/adtp.201700033